DEPARTMENT OF CHEMISTRY, UNIVERSITY OF JYVÄSKYLÄ
RESEARCH REPORT No. 44

ELECTRONIC AND VIBRATIONAL EXCITATIONS IN SOME BIOLOGICALLY RELEVANT MOLECULES

BY
VESA HELENIUS

Academic Dissertation
for the Degree of
Doctor of Philosophy

Jyväskylä, Finland 1993
ISBN 951-34-0160-X
ISSN 0357-346X

DEPARTMENT OF CHEMISTRY, UNIVERSITY OF JYVÄSKYLÄ
RESEARCH REPORT No. 44

ELECTRONIC AND VIBRATIONAL EXCITATIONS IN SOME BIOLOGICALLY RELEVANT MOLECULES

BY

VESA HELENIUS

Academic Dissertation
for the Degree of
Doctor of Philosophy

To be presented by permission of the Faculty of Mathematics and Natural Sciences of the University of Jyväskylä for public examination in Auditorium S-212 of the University on December 18, 1993, at 12 o'clock noon.

Jyväskylä, Finland 1993
ISBN 951-34-0160-X
ISSN 0357-346X

URN:ISBN:978-952-86-0170-8
ISBN 978-952-86-0170-8 (PDF)
ISSN 0357-346X

University of Jyväskylä, 2024

CONTENTS

ACKNOWLEDGEMENTS

This work was carried out at the Department of Chemistry, University of Jyväskylä, during the years 1989-1993.

I would like to thank my supervisor, acting Professor Jouko Korppi-Tommola, for his support during this work. Without his enthusiasm, ideas, criticism and encouragement this work would not have been completed.

Thanks are due to my colleagues Heikki Häkkänen, Raimo Lohikoski (Physics Department), Jukka Siikki, Jari Oksanen, Eira Laitinen, Anu-Sisko Suoranta and Timo Harju for interesting discussions and creating a stimulating atmosphere. I thank the whole staff of the Chemistry Department and especially Sisko Paavola for their kind assistance on many occasions. My special thanks go to Erkki Järvinen and Tapani Sorsa for their invaluable technical help.

Finally, my warmest thanks to my wife Virve for her patience and continuous support during these years. She has had a difficult time organising things with her absent-minded husband and taking care of our little children Aarne and Amanda by herself. I very much appreciate the work she has done.

This research was funded by the Research Council of Natural Sciences of the Academy of Finland.

Jyväskylä, October 1993 Vesa Helenius

LIST OF ORIGINAL PAPERS

This thesis is based on the following original papers. These are referred to in the text by the corresponding Roman numerals.

I. Helenius V. and Korppi-Tommola J., Pico: A data acquisition program for picosecond laser spectroscopy, *Computers Chem.* **16** (1992), 77.
https://doi.org/10.1016/0097-8485(92)85012-N

II. Helenius V., Hynninen P. and Korppi-Tommola J., Molecular structures of chlorophyll *a* aggregates: spectroscopic and molecular modeling study, *Laser Spectroscopy of Biomolecules, Proc. SPIE* **1921**(1993), 86.
https://doi.org/10.1117/12.146105

III. Helenius V., Hynninen P. and Korppi-Tommola J., Chlorophyll *a* aggregates in hydrocarbon solution, a picosecond spectroscopy and molecular modeling study, *Photochem. Photobiol.* **58**(1993) in press.
https://doi.org/10.1111/j.1751-1097.1993.tb04985.x

IV. Helenius V., Siikki J., Hynninen P. and Korppi-Tommola J., Femtosecond relaxation of hydrated Chlorophyll *a* aggregate in hydrocarbon solution, a manuscript submitted for publication in Chemical Physics Letters.
https://doi.org/10.1016/0009-2614(94)00693-8

V. Helenius V., Nieminen J., Kotila S., Korppi-Tommola J., Lohikoski R. and Timonen J. Anomalous temperature dependence of the IR spectrum of polyalanine, a manuscript.
https://doi.org/10.1016/S0009-2614(97)01109-3

ABSTRACT

Chlorophyll *a* (Chla) aggregates in 3-methylpentane solution were studied by pico- and femtosecond absorption and picosecond fluorescence spectroscopy and molecular modeling. Time dependent anisotropies were used to follow rotational diffusion of some of the aggregates. The rotational diffusion of a chlorophyll *a* monomer and (Chla $\cdot 2H_2O)_2$ dimer was hydrodynamic over the viscosity range studied (0.29-1.8 cP). Molecular mechanics calculations were used to predict the minimum energy structures of several chlorophyll dimers suggested earlier in the literature. These structures were used to estimate excitonic splitting of the Q_y-band of chlorophyll *a* and compared to experimentally observed spectral shifts. Femtosecond measurements of a strongly red-shifted large chlorophyll *a*-water aggregate indicated fast 1.5 ps energy transfer and trapping within the aggregate. No indication of exciton annihilation was observed in an excitation intensity range from 7×10^{10} to 1×10^{17} photons/(pulse cm^2).

In the second part of this work a non-linear theoretical model describing energy transfer in α-helical proteins was tested experimentally. The temperature dependence of the infrared spectra of polypeptides tryptophan-$alanine_{15}$ and tyrosine-$alanine_{15}$ was studied. Anomalous red-shifted side-bands in the NH-stretch region were observed. Temperature dependence of the anomalous side-bands was studied by using multivariate principal component analysis. The functional form of the temperature dependence suggests that the anomalous band in crystalline acetanilide at amide-I region and in the polypeptides at NH-stretch region originates from a common mechanism. A non-linear mechanism based on coupling between phonons and a NH-vibration, suggested first by Davydov, seems to explain the temperature dependence. To our knowledge this is the first experimental observation of a soliton in an α-helical polypeptide.

1. INTRODUCTION

Photosynthesis is a chemical reaction where solar energy is used to synthesise carbohydrates from water and carbon dioxide. Practically all energy consumed by living organisms is produced by photosynthesis. Chlorophyll *a* (Chla) is a fundamental molecule of green plant photosynthesis. All organisms capable of oxygenic photosynthesis contain Chla. Chla with some other chromophores give the green plants their characteristic green colour. Chla-protein complexes trap the sunlight in the leaves, transfer the energy to the reaction center and finally form a charge transfer complex in the reaction center. The structures of Chla-protein complexes are still largely unknown because only a few complexes have been crystallised for X-ray diffraction studies[1,2].

In the 1920s it was recognised that the absorption spectrum of Chla is red-shifted in living plants compared to monomeric solutions of Chla *in vitro*. This observation has lead to the preparation of a variety of artificial Chla systems that show similar red-shifts to that of *in vivo* Chla. These systems include adsorbates, micellar systems in solution, thin films and colloidal dispersions[3]. It has been thought that artificial Chla preparations could provide valuable information about the structures and mechanisms that lead to red-shifted chlorophyll species *in vivo*. In most cases the red-shift in the absorption spectrum is induced by aggregation of Chla. Little information about the structures and specific interactions of the aggregates were obtained until the application of magnetic resonance and infrared techniques in the 1960s. Time resolved spectroscopy has opened new possibilities in studies of these complex molecular systems. In this work Chla aggregates have been prepared in hydrocarbon solution. The electronic properties and aggregate structures have been studied by using static and time resolved spectroscopic methods and computer generated molecular models.

Time resolved laser spectroscopy has been an important tool in this research. Development of laser techniques have made it possible to record kinetics of reactions lasting only a picosecond or even less[4,5]. Femtosecond laser pulses are very short. In one second light travels about 300 000 kilometres, in one femtosecond light travels 0.3 micrometers, about one hundredth the thickness of a human hair. The laser pulse can be compared to a shutter of a camera. The faster the movement of the shutter or the shorter the laser flash the faster events can be studied. The femtosecond time range opens some of the fundamental chemical reactions for study[6]. Cleavage of a bond, isomerization reactions of fairly small molecules, energy transfer in photosynthetic systems and solvent relaxation can be followed in real time. In this work ultrafast laser

pulses ranging from 170 fs to 15 ps have been applied to the study of both absorption and fluorescence emission of the Chla aggregates.

In the second part of this work a non-linear theoretical model describing energy transfer in proteins was tested experimentally. The model is worth attention because it would provide a specific mechanism for energy or information transfer in a protein. An energy transfer model for proteins needs to be on the right energy scale. The electronic excitations are too large in energy to be important in physiological conditions. Vibrational excitations are in the right energy range but the lifetime and dephasing time of an ordinary vibration are too short for efficient energy transfer. The model describes a coherent transfer of a vibrational quantum along the hydrogen bond chain inside an α -helix of a protein[7]. The protein could be, for example, a transmembrane protein or a protein in a muscle. Energy that is liberated in the hydrolysis of adenosine triphosphate corresponds to a vibrational quantum of 2500 - 4000 cm^{-1}. The life supporting chemical reactions: biosynthesis, material transport and muscle contraction are driven by ATP hydrolysis. Synthetic polypeptides were used to model proteins. Like proteins, polypeptides are formed from amino acids by peptide bonds. A polypeptide with a specific amino acid sequence can be synthesised. In this work four polypeptides were used: tyrosine-alanine$_{15}$, tryptophan-alanine$_{15}$, glycine$_{25}$-tyrosine and alanine$_{35}$-tyrosine.

Experimental methods applied to polypeptides included low-temperature FTIR spectroscopy and X-ray powder diffraction measurements.

2. EXPERIMENTAL

2.1 Samples

Chlorophyll *a* (fig. 1) was obtained from professor P. Hynninen of the Chemistry Department of University of Helsinki. Chla was prepared by large-scale modification of the method developed by Hynninen[8,9]. The microcrystalline chlorophyll was extremely pure and dry according to NMR- and UV-vis spectra. The solvents 3-methylpentane (3-MP, Fluka) and CCl_4 were dried on activated alumina and stored either on a 4A molecular sieve or (3-MP) on Na.

Different types of Chla samples were prepared for optical measurements. A sample that forms a Chla dimer at low temperatures was prepared by first drying the Chla by co-distillation with dry CCl_4 and then pumping in a 3×10^{-6} mbar vacuum for 30 minutes at 40-50 °C. Then Na-dry 3-methylpentane was added. The procedure results in a solution in which water concentration is sufficiently low for dimer formation. Another sample type is a Chla-water aggregate $(Chla\cdot 2H_2O)_n$ that is formed at room temperature when the Chla/water ratio is bigger than approximately 1/10. These samples were prepared by adding water to the Chla 3-MP solution with a microliter syringe by weight. The Chla/water ratio was adjusted between 1/20-1/40. The water adduct was formed after 1 h of sonication and 2 hours of equilibration. Chla concentration in all the samples were $1\text{-}2\times10^{-4}$ mol/l.

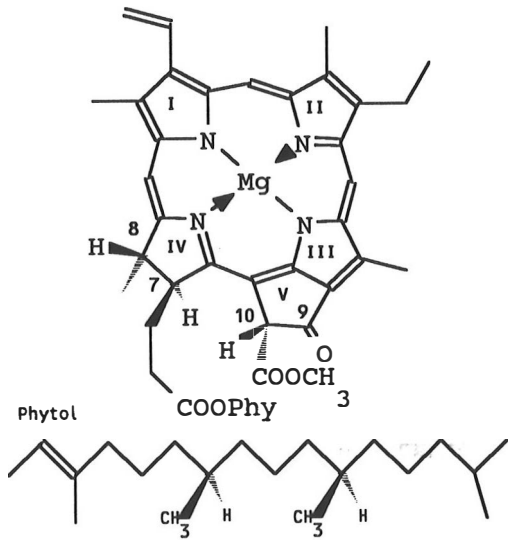

Figure 1. Chlorophyll *a* . The numbering conforms to extended Fischer notation.

The polypeptides tyrosine-alanine$_{15}$, tryptophan-alanine$_{15}$, glycine$_{25}$-tyrosine and alanine$_{35}$-tyrosine were synthesised in the Biochemical Department at the University of Oulu. They were used as received. Acetanilide (ACN) was obtained from E. Merck AG and purified by sublimation.

Samples for low-temperature FTIR-work were prepared by grinding weighted amount of polypeptide or ACN with KBr and pressing tablets with a hydraulic press. The IR spectra were measured on Nicolet 60SX FTIR-spectrometer at 0.25 cm^{-1} resolution in the Department of Physical Chemistry, University of Helsinki. X-ray powder diffraction patterns of the polypeptide samples were measured in capillary with an Enraf-Nonius FR590 Powder diffractometer in the Inorganic Chemistry Department, University of Jyväskylä.

2.2 Picosecond fluorescence measurements

Fluorescence single photon counting is a technique for collecting the time profile of excited electronic state relaxation by following the decay of fluorescence intensity in time. Single photon counting is a very sensitive technique with a large dynamic range and a wide useful wavelength range. The worst shortcoming of single photon counting is the time resolution that is limited to 10-20 ps because of noise from the electronic detection system. Fluorescence single photon counting is a well established technique. The reader is referred to the literature for a more extensive description of single photon counting than is stated here[10,11].

Experimental setup

Figure 2 shows the experimental arrangement used in this study. A picosecond dye laser output was used to excite the sample. The excitation pulse was divided into two parts. One part was detected by a fast avalanche photodiode (RCA C30902) and the pulse from the photodiode triggered a raising voltage ramp in a time-to-pulse height converter (TAC, ORTEC 467). The other part of the pulse was focused into the sample to excite fluorescence. Fluorescence is usually collected at a right angle with respect to excitation. The detection optics consisted of an imaging lens, a cut-off filter and an interference filter. A lens was used to focus the fluorescence onto the detector. A cut-off filter was used to remove scattered excitation light that can be several orders magnitude more intensive than fluorescence. An interference filter was used to select the wavelength region of interest. A calcite polarizer was used to select the detection polarization. Lifetime measurements are generally made at the magic angle polarization (54.7°), where the effect of rotational diffusion is averaged out. Fluorescence was detected by a microchannel plate photomultiplier (MCP, Hamamatsu R1654U-07) with excellent timing characteristics as compared to an ordinary photomultiplier tube. A single photon detected induces an electrical pulse from MCP that is amplified in a separate amplifier. Pulses from the MCP and photodiode are led through constant

fraction discriminators (CFD, Ortec 583) to minimise timing variations resulting from pulse height fluctuations. The MCP pulse stops the voltage ramp of the TAC. The time difference between the diode and MCP pulses determines the output voltage of the TAC. Each single photon event is counted in a channel corresponding to the output voltage of TAC on a multichannel analyser (Nokia LP4700). In order to avoid accumulation of fast events the count rate has to be less than 1% of the excitation pulse repetition rate. In practice a count rate of 0.1% was used. This means that statistics of one million counts can be collected in 20 minutes at 760 kHz repetition rate.

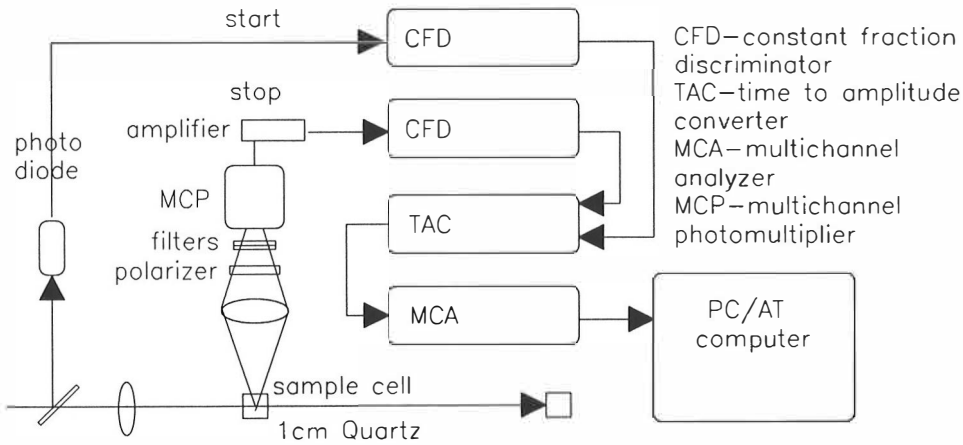

Figure 2. Time-correlated single photon counting experiment.

Signal description

With the present picosecond laser system and detection electronics an instrumental function with full width at half maximum of about 80 ps can be obtained. Instrumental function is the response of the detection system to light scattered from the laser pulse. The fluorescence signal *f(t)* can be described as a convolution of theoretical fluorescence decay *g(t)* and the instrumental function *h(t)*[10].

$$f(t) = \int_0^t h(t-t')g(t')dt' \qquad (2.1)$$

The data analysis of fluorescence decay histograms is usually done with iterative computer convolution of the measured instrument function *h(t)* with some fluorescence decay model *g(t)* until a satisfactory agreement is obtained between the model and the measured curve. In favourable cases very accurate parameters can be obtained if the

model is correct because of good statistics and well known noise characteristics of the experiment.

2.3 Pico- and femtosecond absorption recovery measurements

In the time-correlated single photon counting the time resolution is limited by detection electronics. The absorption recovery method is a technique where the duration of the laser pulses is the factor limiting the time resolution. The experiment is based on the use of two laser pulses: the first pulse (a pump pulse) is used to initiate a photochemical event in the sample, the second pulse (a probe pulse) is delayed in time and used to follow changes in the sample after excitation[5]. A variable time delay between the pulses is accomplished by passing the probe pulse through an optical delay. Optical delay of one femtosecond corresponds to a distance of 0.3 micrometers, which can be obtained by a mechanical translation stage.

Experimental setup

Figure 3 shows the absorption recovery setup. The optical delay line consisted of a mechanical translation stage, stepping motor electronics, a 2 kHz chopper and an EG&G Parc 5209 lock-in amplifier. The experiment was set up during this work. The software, that is described in detail in paper I, operates by initiating the stepping motor controller to move the delay mirror over the desired optical delay. The measurement is then started and the movement of the translational stage is followed by a pulse counter card. The time delay is divided in 1024 positions where the data is collected from the lock-in amplifier via the GPIB bus. After the measurement the translational stage is programmed to move back to its original position. Data is saved on the hard disk of the controlling IBM PC/AT computer and displayed graphically on the screen. The delay line can also be controlled manually by a joystick for alignment purposes. The software was written in the C-programming language.

A modified version of the software, designed for the picosecond experiment, was used for femtosecond experiments. In the modified scheme the stepper motor control electronics and mechanics were assembled for shorter step size and the operation principle was changed from continuous movement of the translation stage to a periodic movement where the carriage is stopped at each point of delay where the signal is to be read from the lock-in amplifier. A 1 kHz repetition rate of the amplified femtosecond system required a new chopper with 10-100 Hz chopping frequency. The setup is presented in the figure 3.

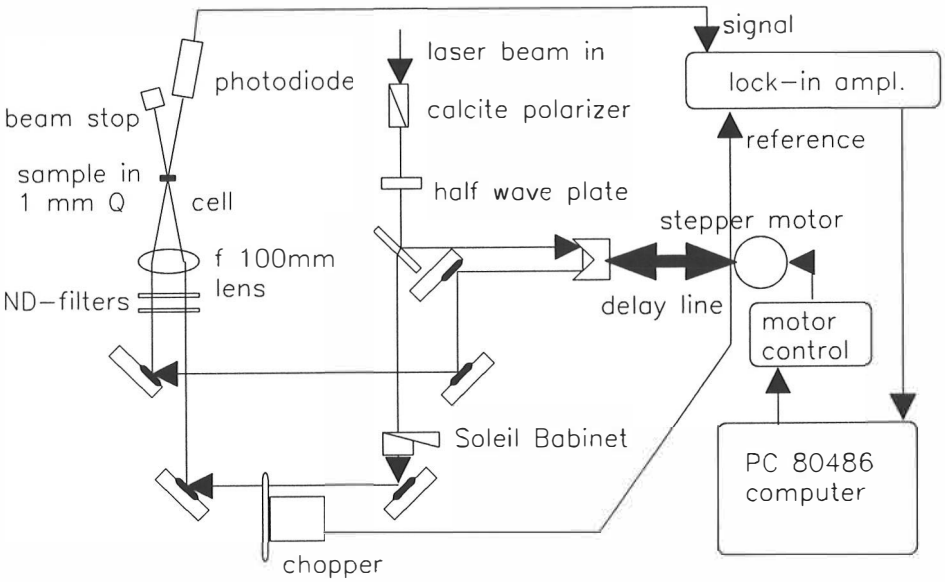

Figure 3. Absorption recovery measurement setup.

Absorption recovery signal

With use of high repetition rate laser excitation a lock-in amplifier detection can be used. In this technique the pump beam is mechanically chopped and a lock-in amplifier is used to detect the modulation of the probe beam at chopping frequency. Assuming that the probe does not change the ground state population significantly the bleaching after strong excitation pulse is[12]

$$\frac{\partial}{}i(x,t) \quad -\sigma i\,(x,t)(N-\Delta N(I(x,t),t)) \tag{2.2}$$

where $i(x,t)$ is probe intensity, $I(x,t)$ is excitation intensity, t is time, σ is the absorption coefficient, N is the ground state population density and $\Delta N(I(x,t),t)$ is the intensity dependent change in ground state population. After integrating over sample depth d eq. 2.3 is obtained.

$$i(t-t_0) = i_0(t-t_0)\exp(-\sigma d(N-\langle \Delta N(t)_x \rangle)) \tag{2.3}$$

where t_0 is time delay between pump and probe pulses and $\langle \Delta N(t)_x \rangle$ is the bleaching of the ground state population averaged over the sample depth. Assuming a δ-function excitation and a small change in the ground state population the equation 2.3 can be expanded

$$i(t-t_0) = i_0(t-t_0)e^{-\sigma dN}(1+\sigma d\langle \Delta N(t)\rangle_x) \tag{2.4}$$

where the $i_0(t\text{-}t_0)\exp(\text{-}\sigma dN)$ term represents the transmitted probe intensity without excitation. By using a mechanical chopper and lock-in amplifier detection only the difference between transmitted probe intensity with and without pump is detected:

$$\frac{i(t-t_0) - i_0(t-t_0)e^{-\sigma dN}}{i_0(t-t_0)e^{-\sigma dN}} = \sigma d\langle \Delta N(t)\rangle_x. \tag{2.5}$$

If a direct detection with photodiodes is used, the signal is more conveniently expressed as

$$\frac{i(t-t_0)}{i_0(t-t_0)} = e^{-\sigma dN} + e^{-\sigma dN}\sigma d\langle \Delta N(t)\rangle_x \ . \tag{2.6}$$

2.4 The laser systems

Two different laser systems have been employed in this work. An Ar^+-ion pumped picosecond dye laser that represents the technology of the 1980s was used to generate picosecond pulses for the single photon counting experiment and for the absorption recovery experiment at picosecond time resolution. A second laser system was based on an amplified Ti:Sapphire ($Ti:Al_2O_3$) laser that became commercially available in 1992. Ti:Sapphire is a solid state laser medium with a very broad useful bandwidth in the near infrared region (720 - 1100 nm). Ti:Sapphire has proven to be invaluable in producing femtosecond laser pulses that were used for absorption recovery experiment in this work.

Picosecond laser

In the picosecond laser system the pump laser is an actively mode locked Ar^+-ion laser. It produces a 76 MHz pulse train of 150 ps pulses at 514.5 nm (Coherent Innova 15 W Ar^+-ion laser, 486-AS mode-locker). Modelocked output power used for pumping of the dye laser is 600 mW. Modelocking is accomplished by electro-optically modulating the gain of the laser resonator at the cavity resonance frequency. The 76 Mhz pulse train is used to synchronously pump a dye laser (Coherent CR-599-04). A cavity dumper (Coherent Inc., Cavity Dumper 7200) was used to select the dye laser output repetition rate. A typical average output was 5 mW at repetition rate of 760 kHz.

Laser pulses of 10-15 ps were readily obtained with DCM (605-690 nm) and LDS698 (670-730) laser dyes (Exciton Inc.).

Amplified femtosecond laser

The femtosecond laser system is based on several new concepts of laser design: Ti:Al_2O_3 laser medium, nonlinear Kerr-lens modelocking[13] and regenerative chirped pulse amplification[14,15]. One year after the first laboratory reports of this laser type in 1991 the equipment became commercially available. The system consists of a seeder laser that produces femtosecond pulses for amplification, a stretcher-compressor unit and a regenerative amplifier.

The seeder laser is a Coherent Mira 900-F Ti:Sapphire femtosecond laser. The laser is pumped by 12 W multiline continuous wave output from a stabilised Coherent Innova 400 15W Ar^+-ion laser. The femtosecond cavity consists of seven mirrors, a Ti:Sapphire crystal, a pair of compensation prisms, a starter mechanism, a tuning element and an adjustable slit. The novelty in design of Mira is the mechanism of modelocking. Modelocking is achieved by utilising the optical Kerr effect where index of refraction of the medium is intensity dependent. The laser cavity is designed to offer a better gain for a beam with small diameter. Normally only one or two longitudinal modes are sustained in the Mira cavity. To form a Kerr lens in the Ti:sapphire crystal high intensity is required. This high intensity can be achieved by random fluctuations of large numbers of longitudinal modes. The modes are generated in the laser cavity by rapidly changing the length of the laser cavity by a starter mechanism. Once the Kerr lens is formed in the Ti:Sapphire crystal and the modelocking started the cavity amplifies preferentially high intensity modelocked pulses capable of forming a Kerr lens in the crystal. Femtosecond pulses of 100 - 200 fs are obtained by compensating the group velocity dispersion of the cavity by a pair of prisms with normal and anomalous dispersion. Mira produces a 1.5 W output at 76 MHz repetition rate. The useful wavelength tuning range is 720 - 990 nm.

A Quantronix 4820 stretcher-compressor unit is used to stretch the femtosecond pulses for amplification. Stretching into the hundred picosecond region is obtained by introducing a frequency chirp in the laser pulse by a grating pair. In a chirped laser pulse the frequencies of the wave packet are spread in time. In a positively chirped pulse the low-frequency components lead the high frequency components. By a symmetric grating pair a chirped pulse can be compressed back to its original width[13,14]. The stretched pulse is fed into a regenerative Ti:Sapphire amplifier that

amplifies the pulse by a factor of 40000. Without stretching the peak intensity would be too great for amplification. The amplifier operates at 1 kHz repetition rate. Sophisticated timing electronics synchronises the amplification with pulses of the Mira and the output of the Nd:YLF laser. The amplifier is pumped by 8 Watts of Q-switched and frequency doubled output of a Quantronix 527 Nd:YLF laser. The amplified pulse is compressed in the stretcher-compressor unit back to a 200 fs pulse. An average output of 500 mW is obtained at 800 nm. Peak power of a 500μJ laser pulse lasting 200 fs is 2.5 GW.

3. CHLOROPHYLL *a* AGGREGATES

An understanding of non-covalent interactions of Chla with external nucleophiles and other Chla molecules would make a significant contribution to an understanding of interactions in Chla-protein complexes. Chla has several active sites for Chla-ligand and Chla-Chla interactions. These include the central Mg-atom, the carbonyl group C9 and the ester C=O oxygens on C13 methyl ester side chain and C17 propionate side chain (fig. 1). A hydrocarbon solvent is not solvating the porphyrin macrocycle of Chla very well, and Mg of Chla in hydrocarbon solution readily co-ordinates to nucleophilic molecules containing S, N or O with lone pair electrons. The C=O groups of Chla form hydrogen bonds in nonpolar solution[3,16].

Chla in 3-methylpentane with variable amount of water shows remarkably complex aggregation behaviour. In a very dry solution different types of aggregates are formed compared to wet solution[17]. The aggregate formation is strongly temperature dependent. Aggregation is clearly manifested in the visible absorption and fluorescence spectra of the solutions. Figure 4 shows absorption spectra of a dimer forming solution at room temperature and low temperature and spectra of a solution containing 20×more water than Chla.

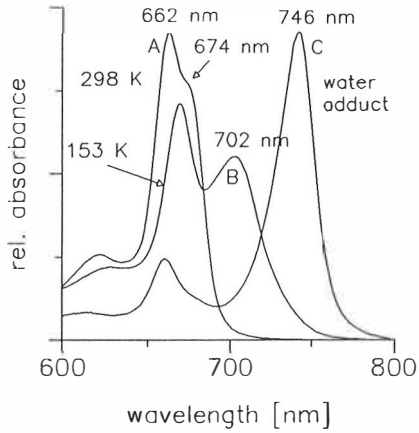

Figure 4. Absorption spectra of Chla in 3-methylpentane solution with variable amount of water. **A)** A solution with stoichiometric amount of water at room temperature. **B)** The same solution at 153 K. **C)** A solution with Chla/water ratio 1/40.

The aim of this work was to study both the structure and electronic properties of these Chla aggregates. In the literature various structural models can be found that are based on results obtained by different experimental techniques. These models were evaluated on the basis of time-resolved studies and computer generated molecular models. Molecular exciton theory was used to estimate excitonic red shifts of each dimer model. The modeling work and exciton calculations are described in papers II and III.

3.1 Theory

Exciton model

The red shift of Q_y-band observed in the aggregated Chla solution originates partly from interaction of the transition moments of the molecules in the aggregate and partly from the bonding interactions between the chromophore units. Molecular exciton theory is a state interaction theory that can be used to estimate the changes in the absorption spectrum due to interaction of transition moments of molecules in an aggregate[18-21]. In the simplest model the transition moments are approximated as dipoles.

The dimer energies are calculated perturbationally. A strong coupling case, where the intermolecular electronic interaction is large compared to intramolecular electron-nuclear coupling is assumed. Molecular exciton theory leads to the following characteristic expression for the transition energy splitting of a dimer:

$$E_{\text{dimer}} = E_{\text{monomer}} + \Delta D \pm \Delta E \tag{3.1}$$

where E_{dimer} is the transition energy for the dimer, E_{monomer} is the corresponding energy for the monomer, ΔD describes the environmental shift of the ground state energy and ΔE is the transition energy splitting. In the point-dipole approximation the exciton splitting term becomes:

$$\Delta E = \frac{\vec{\mu}_i \cdot \vec{\mu}_j}{R_{ij}^{\,3}} - 3\frac{(\vec{\mu}_i \cdot \vec{R}_{ij})(\vec{\mu}_j \cdot \vec{R}_{ij})}{R_{ij}^{\,5}} \tag{3.2}$$

where $\vec{\mu}_i$ is the transition dipole moment vector in molecule i and $\vec{R}_{ij}$ is the position vector between the two dipoles. In Chla the transition dipole vector for the Q_y transition lies approximately along the N(I)→N(III) axis (fig 1). A transition dipole strength of 5.16 Debye was used for the exciton calculations[22].

Hydrodynamic model

The rate of diffusion of a molecule in solution depends on the size and shape of the molecule and the solvent viscosity. Therefore the rotational diffusion rate is a useful property for estimating relative sizes of aggregates. The rate of rotational diffusion of a dye molecule can be measured either by time resolved fluorescence anisotropy or by

anisotropy of ground state recovery. The anisotropy is measured by analysing the signal at parallel polarization and perpendicular polarization with respect to excitation. The anisotropy function *r(t)* is defined as

$$r(t) = \frac{I_{\parallel}(t) - I_{\perp}(t)}{I_{\parallel}(t) + 2I_{\perp}(t)} \tag{3.3}$$

where $I_{\parallel}$ is signal measured at parallel polarization and $I_{\perp}$ is signal measured at perpendicular polarization.

The simplest model describing rotational diffusion in solution is the Stokes-Einstein-Debye model that assumes a spherical solute in a continuous solvent medium[23]. In this model the microscopic viscosity is approximated by macroscopic viscosity of the solvent. Recent ultrafast studies of isomerization reactions and rotational diffusion of small molecules indicate that, especially when the solute size is close to size of the solvent molecules (or smaller), the microscopic viscosity is different from the macroscopic one[24-26]. The assumption of a spherical solute is also a limitation of the SED model.

As Chla is a highly asymmetrical molecule, any conventional hydrodynamic model (a sphere or an ellipsoid) hardly gives an accurate description of the rotational diffusion of Chla aggregates in solution. A more flexible model was used in this work[27]. In this model rotational diffusion time is proportional to the rotational friction coefficient, $\tau_r = B\zeta$, where the coefficient B includes size and shape of the diffusing molecule. The frictional coefficient ζ is proportional to the shear viscosity, η, of the solvent,

$$\zeta = (\eta k_B T)\xi \tag{3.4}$$

where coefficient ξ measures the relative variation of the microscopic friction from its macroscopic value $(0 \le \xi \le 1)$. In the hydrodynamic limit (ξ=1) the rotational correlation time is

$$\tau_r = \frac{B\eta}{k_B T} \tag{3.5}$$

We assume that for Chla aggregates in 3-MP solution the boundary condition is independent of the type of the aggregate. Because of the large size of the Chla molecule as compared to the solvent molecules the stick boundary condition is expected to be valid (ξ=1). For aggregates being even larger the boundary condition

should be preserved. The shape factors that are also included in the constant B are assumed to be the same for the monomer and for sandwich structured dimers. Under these assumptions the constant B is directly related to the relative size of an aggregate.

Molecular modeling

Molecular modeling work was done on a Silicon Graphics PERSONAL IRIS 4D/35 TG+ workstation. Molecular Simulations QUANTA modeling software was used. Molecular mechanics calculations were used to build the aggregates. In molecular mechanics each atom and bond type is parametrized to have certain bond angles, distances, dihedral angles and charge distribution. Solvent screening of the Coulombic interactions is taken into account by using a distance dependent dielectric factor. The parameters define a force field that determines the shape of the molecule. The aggregate structures were minimised by using the CHARMm force field[28]. Minimisation of a large aggregate like a Chla aggregate is a minimisation on a very complicated potential surface. No method exists for finding the absolute minimum energy conformation of such a surface in a reasonable calculation time. Therefore the obtained structures always represent some local minimum of the conformational space. Ethyl chlorophyllide *a* was used instead of Chla for modeling of aggregates to simplify the calculation. The standard parametrization of QUANTA/CHARMm was used with the exception that two covalent bonds (2.086 Å) were introduced between the porphyrin ring nitrogens and the central magnesium. The bond length was taken from the X-ray crystal structure of ethyl chlorophyllide *a*[29]. The magnesium atom lies in the porphyrin plane in the minimised monomer structure. In the aggregates planarity of the porphyrin moieties is preserved. In solution the conformation of Chla depends on the co-ordination of the magnesium atom. In this respect the bond constraints restrict the conformational freedom of the porphyrin ring. It wasn't considered as a severe limitation. For example, in the crystal structure of the ethyl chlorophyllide *a* the magnesium atoms lies 0.4 Å above the porphyrin plane. The distance dependent dielectric factor was used to represent the solvent effect on electrostatic interactions. The charges of the most important atoms were Mg +1.98, porphyrin ring N -0.42, carbonyl C=O -0.60, ester C=O -0.57 and ethereal —O— -0.67.

3.2 Results

Time resolved studies

A usual trend in the Chla aggregates is that as the coupling between the chromophores and size of the aggregate increases the electronic lifetime decreases and the fluorescence quantum yield decreases. Within one solvent and temperature the electronic lifetime changes from a 6.3 ns lifetime of Chla·$2C_5H_5N$ (Chla - pyridine complex) to a 1.5 ps lifetime of $(Chla·2H_2O)_n$ water adduct. Results from the fluorescence and absorption recovery experiments are collected in Table 1. The representation $(Chla·2H_2O)_n$ etc. used to characterise different Chla species is meant to clarify the type of the aggregate, not to indicate an exact stoichiometry. It follows the usual notation used in literature. Time resolved studies are included in paper III. The femtosecond results of the Chla-water adduct are described in paper IV.

In spite of overlapping absorption and fluorescence spectra different species are easily identified by their characteristic lifetimes. Monomeric Chla shows a single exponential excited state lifetime of the order of 5-6 ns both in 3-methylpentane solution containing other Chla species and in a solution containing only the Chla-pyridinate complex. A slight shortening of the lifetime in the solution containing aggregated Chla indicates energy transfer from monomeric Chla to aggregated Chla. A 702 nm absorbing species that is considered to be a dimer $(Chla·2H_2O)_2$ shows a 2-2.5 ns lifetime that is about one half of the lifetime of the monomeric Chla. The lifetime agrees well with lifetime shortening caused by enhanced radiative and intersystem crossing rates predicted for a dimer[30] on the basis of exciton theory. The $(Chla)_n$ aggregate absorbing at 674 nm can not be described as a strongly coupled excitonic system. The fast 18% fluorescence lifetime component observed at 656 nm is 0.7 ns. The corresponding fast component observed at 736 nm is 1.0 ns. This indicates that energy transfer is taking place between donor and acceptor molecules of the aggregate. The $(Chla·2H_2O)_n$ water adduct is different from the other aggregates. The red shift of the Q_y-absorption band is large (1650 cm^{-1}) and the observed excited state kinetics are very rapid. It shows a strong circular dichroism signal (V. Helenius, unpublished data) indicating a strong exciton interaction between molecules of the aggregate. The aggregate tends to reach colloidal dimensions that appear as crystal-like precipitation when an excess of water is added in to the solution. An ink-like precipitation is observed when only 20-40 times excess of water is present. The light scattered from the microscopic particles created technical difficulties in pump-probe measurements of this sample. The water adduct showed a constant 1.5 ps absorption recovery lifetime within experimental error over

Table 1. Time resolved data on Chla aggregates in 3-methylpentane solution at room temperature. Under a heading 'Species' the type of Chla aggregate is indicated, excitation wavelength λ_{exc} (emission wavelength λ_{em}), electronic lifetime τ and decay time of anisotropy $\tau_{r(t)}$.

Absorption recovery

Species	λ_{exc} [nm]	τ [ps]	$\tau_{r(t)}$ [ps]
Chla·$2C_5H_5N$	662	$(4.4\pm0.5)\times10^3$	150±20
$(Chla)_n$	674	$(1.0\pm0.1)\times10^3$	250±40
*$(Chla\cdot H_2O)_2$	702	$(2.5\pm0.5)\times10^3$	680±120
$(Chla\cdot 2H_2O)_n$	743	1.5±0.3, 35±5	1.5±0.5

Fluorescence lifetimes

Species	λ_{exc} [nm]	λ_{em} [nm]	τ [ns]
Chla·$2C_5H_5N$	580	675	6.3±0.1
Chla·H_2O	620	656	5.0±0.1
**$(Chla)_n$	620	656	0.7±0.1
*$(Chla\cdot H_2O)_2$	620	736	2.0±0.5
$(Chla\cdot 2H_2O)_n$	620	753	~0.001

*Measured at 248 K

**Fast 18% lifetime component of 656 emission.

excitation intensities from 4.2×10^{14} to 1.0×10^{17} photons/(pulse cm^2). This behaviour is strikingly different compared to the exciton annihilation processes that are observed in some dye aggregates with strong exciton coupling[31-34]. The kinetics showed another lifetime component of about 35 ps and a long lifetime component >100 ps that could not be accurately determined by absorption recovery measurement. Fluorescence lifetime measurements gave two lifetime components of about 1 ps and 3.9 ns over excitation intensities from 7.1×10^{10} to 9.0×10^{13} photons/(pulse cm^2). The absorption recovery experiment gave a 1.5 ps anisotropy decay time indicating that energy transfer within the aggregate causes the fast initial decay. Anisotropy decay starts from value r(t)=0.4 and decays in 1.5 ps to a value r(t)=0.25 that stays constant over the useful observation range of about 100 ps.

The sizes of the aggregates were studied by recording the anisotropy decay times at different temperatures (100-298 K, viscosities 0.29-1.8 cP). In the aggregates where no significant energy transfer takes place the anisotropy decay time can be related to the relative size of an aggregate by eq. (3.5). In this case the anisotropy decay is due to rotational diffusion only. As rotational diffusion times were plotted against η/T it was observed that the rotational correlation time of $(Chla{\cdot}H_2O)_2$ increased twice as fast as the correlation time of monomeric Chla ($Chla{\cdot}H_2O$ or $Chla{\cdot}2C_5H_5N$). This is a good experimental proof for a widely agreed assignment that the species absorbing at 702 nm is a dimer. An even faster increase in rotational correlation time was observed for the $(Chla)_n$ aggregate absorbing at 674 nm. Interpretation of this band is not as straightforward as that of the dimer band. Assuming a rigid aggregate structure the temperature dependence of rotational diffusion would indicate that the 674 nm absorbing species is a trimer. The rotational diffusion appears to be about three times slower than that of the monomer. The molecular modeling results for this aggregate leave a possibility of internal motion in the aggregate as a source of anisotropy decay. The time resolved measurements indicate that the excited state kinetics contain a significant contribution of energy transfer. These complications may invalidate the assumptions of eq. (3.5).

Molecular models

At low temperature in 3-MP solution containing a suitable amount of water, Chla forms a water bound dimer absorbing at 702 nm. The structure of this dimer has been subject to extensive discussion. Molecular mechanics calculations were used to critically compare the different structures suggested for this dimer by Shipman[22] *et al.*, Fong[35] and Abraham[36]. The models were further tested by using molecular exciton theory to predict exciton splittings of absorption bands and comparing these to the observed spectral shifts.

In the proposed structures hydrogen bonded water molecules link the chlorophylls of the dimer together. In the Fong dimer[35] the water forms hydrogen bonds between the C10 C=O methoxycarbonyl groups (fig.1) and the Mg atoms of adjacent molecules. The minimised structure has C2 symmetry. The transition dipoles of the two chlorophylls lie in parallel planes but are oriented perpendicularly with respect to each other. Despite the unfavourable orientation the transition coupling in this structure remains fairly strong because of the short 6 Å distance between the interacting dipoles. Abraham *et al.*[36] suggested a water bound dimer structure based on NMR complexation shifts and ring current calculations. In the suggested model the

chlorophyll planes were parallel. In the computed structure they are tilted about 16 degrees with respect to each other. In this dimer a hydrogen bond is formed between the C9 C=O keto oxygen of the first Chla and a water molecule that is further co-ordinated to the Mg atom of the second Chla molecule. The C=O group of the C7 propionate side chain (fig. 1) of the second Chla is co-ordinated to the Mg atom of the first Chla.

In both Fong and Abraham models the exciton interaction is weak compared to the experimentally observed red shift. In particular, the exciton shift of 38 cm^{-1} calculated for the Abraham model does not account for the observed 861 cm^{-1} red shift. The infrared spectra of the water bound dimer shows that the C9 C=O group is involved in the bonding of the dimer[17]. The pyrochlorophylls also show similar aggregation behaviour despite the fact that they are missing the C10 C=O group which is the bonding group in the Fong dimer[37]. Therefore we conclude that neither the Fong nor the Abraham model is the correct structure for the 702 nm absorbing dimer.

Finally, a structure suggested by Shipman *et al.*[22] was modeled. In the Shipman model, two Chla molecules are symmetrically linked together by two water molecules. Each water molecule is hydrogen bonded to the C9 C=O oxygen of the Chla molecule and the oxygen of the water is co-ordinated to the Mg-atom of the adjacent Chla molecule. The chlorophyll planes are parallel to each other, but are inverted and rotated 180° about the Z-axis and shifted so that pyrrole rings III are approximately on top each other. The structure has C2 symmetry. In the Shipman model the chlorophylls are about 4Å apart but shifted some 8Å with respect to each other. Molecular mechanics calculations showed that there are no close contacts in the Shipman dimer and that the structure is easily obtained without any strict requirements for positions of the side chains. The exciton shift obtained for the Shipman model (242 cm^{-1}) is comparable to the experimentally observed red shift 861 cm^{-1}, assuming an environmental shift of the order of 600 cm^{-1}. This size of environmental shift has been shown to be consistent with the shift needed to predict the absorption of the crystalline monolayer of methyl chlorophyllide *a*, where similar molecular interaction takes place as in the dimer model[18].

The 674 nm absorbing aggregate species is a Chla self-aggregate as it is formed even in extremely dry hydrocarbon solution where no external nucleophiles are present[17]. Chla self-aggregation is known to proceed via bonding of the Chla C9 keto C=O groups to the central magnesium atom. Molecular mechanics calculations were used to study the

models described by Houssier and Sauer[38], Kooyman and Shaafsma[39], Myslinski and Koningstein[40-42], Fong[43], Fong and Koester[44] and Abraham and Smith[45].

A modification of a T-shaped aggregate structure was originally proposed by Houssier and Sauer[38]. It has also been discussed by Kooyman and Schaafsma[39] in their study of nuclear spin relaxation times and NMR shifts of Chla in chloroform. More recently Koningstein[40-42] and co-workers have studied the same species of Chla in hexane solutions using picosecond fluorescence and Raman spectroscopy. According to our molecular mechanics calculation the chlorophyll planes of this dimer are perpendicular to each other and the C9 C=O oxygen of one Chla co-ordinates directly to the magnesium atom of the adjacent Chla molecule. In this structure there is no structural limitation for the size of the aggregate. In the T-shaped dimer one Chla is an electron donor and the other is the acceptor. In a larger aggregate the chlorophylls in the chain act as both electron donors and acceptors.

The experimentally observed red shift of the Chla self aggregate is only 267 cm^{-1}. Therefore, a structure with a weak transition interaction is to be expected. In the T-shaped aggregate the transition dipoles are nearly at right angles with respect to each other resulting in a very weak coupling of the transition dipoles. Exciton calculation gave a shift of 26 cm^{-1} for the dimer structure, that does not account for the experimentally observed red shift. The hydrogen bonding of the C9 C=O oxygen to the magnesium of the acceptor Chla is almost the only conceivable local interaction that could give rise to the observed red shift.

3.3 Conclusions

The time resolved spectroscopic results provided a comprehensive picture of the aggregation taking place in a 3-methylpentane solution. Different models suggested in the literature were evaluated by using experimental data and molecular models. For a Chla dimer $(Chla{\cdot}H_2O)_2$ absorbing at 702 nm, a model suggested by Shipman *et al.*[22] proved to be the most promising model. The rotational correlation time measurements provided experimental confirmation for the assumption that 702 nm species really is a dimer. Exciton calculations of the dimer shifts showed that Shipman model provides reasonable geometry for exciton interaction. The Shipman model is also consistent with other experimental data available. The model compounds and the IR spectrum of the dimer indicate that hydrogen bonding of the C9 C=O group plays a significant role in bonding of the dimer.

A second aggregate type is formed in a dry 3-methylpentane solution. The aggregation proceeds through direct Chla-Chla interactions. The small red-shift from 662 nm to 674 nm indicates weak interaction between the molecules of the aggregate. A model where Chla planes of adjacent molecules are in a perpendicular position with respect to each other explains the experimental observations. The model is asymmetrical. Exciton interaction between the transition moments is very weak in this structure. The red shift originates from the co-ordination of the C9 C=O group of the electron donor to the Mg-atom of the electron acceptor. The structure allows for composing of larger aggregates that could explain the long rotation correlation times observed. The T-shaped structure is also supported by other experimental evidence. It has been shown that the C9 keto C=O group is bonded and the C10 carbomethoxy group is free in Chla self aggregates[46]. In spite of weak excitonic coupling quite short lifetimes were observed for the $(Chla)_n$ aggregate. Energy transfer between the electron donor and acceptor molecules in the aggregate may explain the short lifetimes.

A third species studied was a strongly red-shifted Chla-water adduct $(Chla{\cdot}2H_2O)_n$. It showed quite different excited state lifetime compared to the other aggregates. A 1.5 ps initial lifetime and a 1.5 ps anisotropy decay indicates that fast energy transfer dominates the excited state kinetics. No exciton annihilation effect could be observed over a million-fold change in the excitation intensity.

The molecular modeling combined with time resolved spectroscopy proved to be an effective method of characterising aggregates of Chla. In the future, molecular dynamics simulations will be used to study the aggregates because of the large conformational space and the dynamic nature of the aggregates. A simulation work has already been started on monomeric Chla in hydrocarbon solution. A second improvement for the current work would be to use more realistic theoretical models for excitonic calculations. The Chla molecule contains conjugated bonds and the electronic orbitals are delocalised over the porphyrin ring. In the Chla aggregates the intermolecular distances are short. A multipole treatment of the transition dipoles could yield more accurate results in this kind of system. The very strong CD-signal of the Chla-water aggregate (V.Helenius, unpublished data) provides further experimental data for theoretical considerations.

4. POLYPEPTIDES

Co-ordinated motion is an essential feature of life. It is known from biochemistry that hydrolysis of ATP leads to conformational changes in molecules taking part in generation of mechanical work[47]. A muscle contraction is driven by coherent sliding of thin and thick protein filaments past each other. Thick muscle fibre consists mainly of protein called myosin. Myosin protein contains a long (0.13 μm) part which is a double coil made of two identical α-helices entwined together. No definite model for the mechanism of muscle contraction exists. This problem illustrates the need for a theoretical model that would explain the coherent transfer of energy liberated in hydrolysis of ATP (2500-4000cm^{-1}) to the site where reaction takes place[48].

A.S. Davydov and N.I. Kislukha[7] suggested in the early 1970s a nonlinear theoretical model describing vibrational energy transfer in α-helical proteins. First experimental evidence on "solitons" (self trapped vibrational state) in a real molecular system came from observations of anomalous temperature dependence of intensity of C=O vibration of crystalline acetanilide (ACN)[49]. The soliton model was the best explanation for the unusual temperature dependence of amide-I vibration. ACN is an interesting molecule because the hydrogen bonded network in the crystal is nearly identical in bond angles and distances to hydrogen bonds inside the α-helix of a protein. In this work, the question as to whether these nonlinear excitations can be found in protein-like molecules is addressed. The temperature dependence of IR-spectrum of four synthetic polypeptides was studied and reported in paper V.

4.1 Theory

The α-helical structure of protein is determined by three hydrogen bonded chains inside of the helix. The chains are formed from hydrogen bonds …C_α—C=O···H—N—C_α—C=O···H—N—C_α… interconnecting peptide units of adjacent turns of the helix (C_α represents α-carbon of a peptide unit). The idea of the Davydovs soliton model is that vibrational energy (for example C=O stretching vibration) is transferred along the chain in a form of a self-trapped wavepacket[7]. A sound wave propagating along the helix is coupled to the excitation and co-operation of the excitation and the sound wave results in a wave packet with small dispersion. The interaction between the three hydrogen bonded channels is assumed to be small. Theoretical studies and experimental results on ACN have lead to variations of the original Davydov model[50-58].

The Davydov model Hamiltonian can be expressed as[59]

$$\hat{H} = \sum_m \Big\{ E_0 \hat{B}_m^+ \hat{B}_m - J\left(\hat{B}_{m+1}^+ \hat{B}_m + \hat{B}_{m-1}^+ \hat{B}_m\right) + \frac{\hat{p}_m^2}{2M} + \frac{\omega}{2}(\hat{u}_m - \hat{u}_{m+1})^2 + \chi_a(\hat{u}_{m+1} - \hat{u}_{m-1})\hat{B}_m^+ \hat{B}_m \Big\} \tag{4.1}$$

where operators $\hat{B}_m^+$ and $\hat{B}_m$ create and annihilate excitation in the peptide group m, the $\hat{u}_m$ operator describes displacement of the peptide group m from its equilibrium position, $\hat{p}_m$ is the momentum operator of the sound wave, E_0 is the energy of the vibration, J is dipole-dipole interaction energy of neighbouring dipoles, M is a mass of one peptide group, ω is the spring constant of the displacement of the peptide group and χ_a is a coupling constant between the longitudinal displacement and vibrational excitation.

Theoretical[60-62] and numerical analyses[62,63] of the solutions of the Davydov model have shown that at certain intervals of parameters a solitary wave solution is achieved. This has been proven to be true at zero-temperature. The parameters are considered to be realistic for a real α-helix. A question whether the soliton can survive at physiological temperatures is still open.

4.2 Results and discussion

Crystalline ACN shows a strongly temperature dependent absorption band at 1650 cm^{-1}. The intensity of the carbonyl stretching mode (amide I) at 1665 cm^{-1} is inversely proportional to the intensity of the 1650 cm^{-1} peak. The soliton model has provided an explanation for the temperature dependence of the intensities of these peaks. Amide I vibration is not the best possible candidate for energy transfer in proteins. The energy of amide I vibration is too small (approximately by a factor of two) when compared to energy liberated in ATP hydrolysis. A more promising candidate would be N-H stretching vibration that is on the right energy scale (3200 -3400 cm^{-1})[64]. The N-H bond is an integral part of the hydrogen bonded chain inside an α-helix in a similar way that the C=O bond is.

The IR spectrum of the amide I region of the microcrystalline ACN sample was measured in the temperature range from 11 to 240 K. The spectrum in this region consists of two absorption bands centred at 1650 cm^{-1} and 1666 cm^{-1}. These two

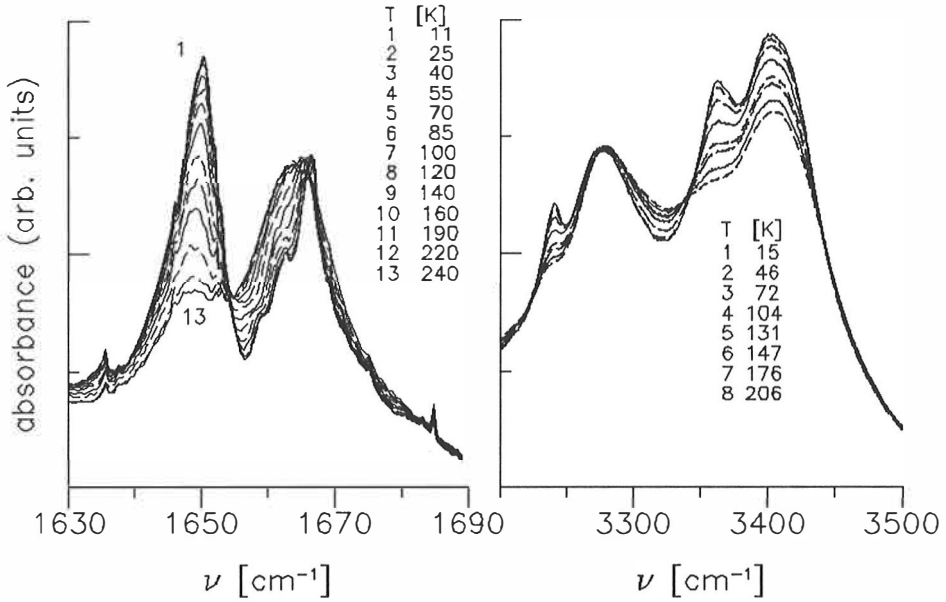

Figure 5. A) The amide-I region of the IR absorption spectrum of ACN at different temperatures. B) The NH-stretch region of the IR spectrum of Trp-Ala_{15} for eight different temperatures.

bands showed complementary behaviour as temperature was lowered. The 1650 cm^{-1} band increased in intensity upon cooling while the intensity of the 1666 cm^{-1} band decreased. An isobestic point was observed at 1655 cm^{-1}, indicating the presence of two transitions at temperature dependent equilibrium (Fig 5A).

The equilibrium of the absorption bands was studied by using multivariate statistical techniques. Principal component analysis[65] (PCA) can be applied to this kind of equilibrium assuming that the positions and shapes of the absorption bands does not vary too much. PCA analysis does not imply any specific band shape as other curve fitting techniques do. It is also insensitive to the shape of the background because only the changing part of the curve is analysed. PCA analysis of the ACN data showed that 96.1% of the total temperature variation of the 1630-1690 cm^{-1} spectral region could be explained by using the first principal component. This component consists of one asymmetrical band at 1650 cm^{-1}, a band centred at 1660 cm^{-1} and an additional band at 1664 cm^{-1}.

In the NH-stretch region of ACN an absorption band with temperature behaviour similar to that of the 1650 cm^{-1} band was observed at 3250 cm^{-1}. This band has been assigned to the first overtone of the 1650 cm^{-1} band by Careri *et al.*[49] Variations of band widths and peak positions as temperature was changed made quantitative analysis of this spectral region difficult.

The low temperature measurements of the polypeptides Trp-Ala_{15} and Tyr-Ala_{15} showed no intensity changes or no new absorption bands in the amide-I region between 15 and 300 K. In the NH-stretch region the situation was quite different. The IR spectrum of polypeptide Trp-Ala_{15} (Tyr-Ala_{15}) showed two broad absorption bands at 3277 cm^{-1} and 3409 cm^{-1} (3272 cm^{-1} and 3412 cm^{-1}). Both bands have weaker, red-shifted and strongly temperature dependent sidebands (Fig. 5B) that appear at 3238 cm^{-1} and 3360 cm^{-1} for Trp-Ala_{15} (3238 cm^{-1} and 3358 cm^{-1} for Tyr-Ala_{15}). In case of longer polypeptides Gly_{25}-Tyr and Ala_{35}-Tyr no significant temperature dependence of the IR spectra were observed in the amide-I region or in the NH-stretch region. X-ray powder diffraction measurement revealed that the longer polypeptides were amorphous while the shorter polypeptides were mainly crystalline with some amorphous material. The two short polypeptides showed a characteristic[66] α-helix IR-absorption at 520 cm^{-1} region. Thus it seems that the anomalous changes in the IR spectrum are characteristic to α-helical polypeptides. The low temperature (140 K) X-ray powder diffraction was used to exclude the possibility of changes in crystal structure at low temperature that could lead to temperature dependent changes in the infrared spectrum.

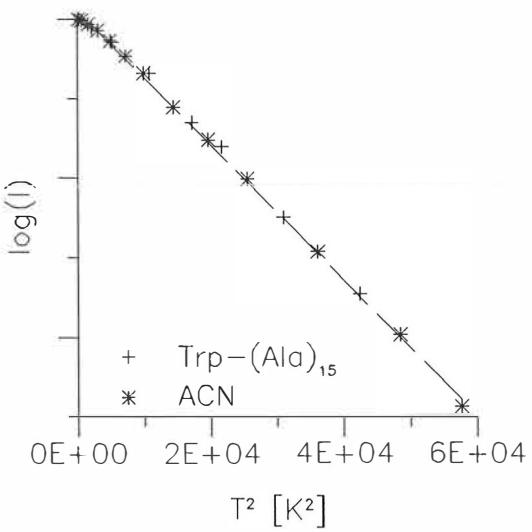

Figure 6. Logarithm of the integrated intensity as a function of temperature squared of the 1650 cm^{-1} band of ACN and of the two red-shifted side-bands in the NH-stretch region of Trp-Ala_{15}. Dashed line is a least square fit to the data points.

PCA analysis of the anomalous bands in the NH-stretch region of polypeptides gave essentially identical temperature dependence for the intensities of the ACN 1650cm^{-1}, Trp-Ala_{15} 3238 cm^{-1} and Tyr-Ala_{15} 3360 cm^{-1} absorption bands. This result suggests that all these bands result from a similar mechanism. If the observed temperature dependence arises from coupling to acoustic lattice modes, the temperature dependence of the integrated intensities of the bands should be proportional[54,55,57] to $\exp(-aT^2)$, where a is constant. Figure 6 shows that this is indeed the case.

Previous results indicate that in IR spectra of polypeptides the NH-stretch mode is mixed with the first overtone of an amide vibration[67-69] to produce two bands in the 3200-3300 cm^{-1} region by the Fermi resonance mechanism. The appearance of two red-shifted anomalous bands can also be explained by Fermi resonance. A Fermi resonance calculation for two nearby bands centred at frequencies ν_A^0 and ν_B^0 leads to two observed bands at frequencies ν_A and ν_B such that

$$\begin{aligned} \nu_A^0 &= (1+I_R)^{-1}(\nu_A + I_R\nu_B) \\ \nu_B^0 &= (1+I_R)^{-1}(I_R\nu_A + \nu_B) \end{aligned} \tag{4.2}$$

where $I_R=I_B/I_A$ is the ratio of the integrated intensities of the observed bands. If it is assumed that the two basic bands in the NH stretch region of Trp-Ala_{15} arise through Fermi resonance of two nearly overlapping bands, the equation above shows that the original bands are centred (at T=0) at 3379 cm^{-1} and 3337 cm^{-1}. In the same way the red-shifted sidebands originate from bands at 3257 cm^{-1} and 3343 cm^{-1}. It is evident that the four observed bands arise from a Fermi resonance between the amide overtone at around 3340 cm^{-1} and the NH-stretch at 3379 cm^{-1} and Fermi resonance between the amide overtone and the red-shifted anomalous band at 3257 cm^{-1}. The other polypeptide, Tyr-Ala_{15}, gave similar results. The ratio I_R is independent of temperature at low temperatures as assumed in the derivation of the above equation. At higher temperatures changes in background (mainly OH absorption of water) leads to an apparent temperature dependence of I_R.

According to the calculation above the shift between NH-stretch mode and its 'soliton companion' is Δ=122 cm^{-1}. An approximate treatment of the Davydov model which assumes a completely localised soliton gives $\Delta = \chi^2\omega^{-1} - 2J$, where χ is the coupling strength between NH-stretch and lattice phonons, ω is the spring constant of a hydrogen bond and J is the nearest neighbour transition dipole energy. Assuming[70] J=6 cm^{-1} and 39 $Nm^{-1} < \omega <$ 59 Nm^{-1}, a coupling strength 323 pN $< \chi <$ 396 pN is found to be in agreement with previously estimated coupling strength[64,55].

4.3 Conclusions

The anomalous red-shifted side bands of the NH-stretch mode of polypeptides Trp-Ala_{15} and Tyr-Ala_{15} is a result of coupling between lattice modes and the NH-stretching vibration. A similar coupling to the lattice modes is observed in the amide-I vibration of ACN. The type of lattice modes taking part in the coupling is still unclear. The fact that no anomalous band in amide region is observed in polypeptides suggests

that the lattice modes involved may be different in ACN and polypeptides. It is conceivable that a localised excitation formed by the NH-stretch mode through coupling with lattice modes may be relatively common in helical polypeptides and proteins. To our knowledge this is the first experimental observation of a soliton in a real α-helical structure.

5. REFERENCES

1. J. Deisenhofer and H. Michel, *Chemica Scripta*, **29**(1989), 205.

2. H. Zuber and R.A. Brunisholz in *Chlorophylls*, ed. Hugo Scheer, CRC Press, Boca Raton, Florida 1991, 627.

3. J.J. Katz, M.K. Bowman, T.J. Michalski and D.L. Worcester in *Chlorophylls*, ed. Hugo Scheer, CRC Press, Boca Raton, Florida 1991, 211.

4. J.D. Simon, *Rev. Sci. Instrum.* **60**(1989), 3597.

5. G.R. Fleming, *Chemical Applications of Ultrafast Spectroscopy*, Oxfort Univ. Press, NY 1986.

6.A.H. Zewail, *Science*, **242**(1988), 1645.

7. A.S. Davydov and N.I. Kislukha, *Phys. Status Solidi*, **B 59**(1973), 465.

8. P.H. Hynninen, *Acta Chem. Scand.*, **B31**(1977), 829.

9. P.H. Hynninen and S. Lötjönen, *Synthesis*, (1983), 705.

10. D. O'Connor and D. Phillips, *Time-correlated Single Photon Counting*, Academic Press, London, 1984.

11. J.L. Lacowicz, *Principles of Fluorescence Spectroscopy,* Plenum Press, NY 1983.

12. H.E. Lessing and A. von Jena in *Laser Handbook* vol 3., ed. M.L. Stitch, North Holland, Amsterdam, 1979, 753.

13. Coherent Mira Model 900 Laser, Operators Manual, Coherent® Laser Group, 3210 Porter Drive, P.O. Box 10042, Palo Alto, California 94303.

14. M. Pessot, P. Maine and G. Mourou, *Optics Comm.*, **62**(1987), 419.

15. J. Squier, F. Salin and G. Mourou, *Optics Lett.*, **16**(1991), 324.

16. J.J. Katz, L.L. Shipman, T.M.Cotton and T.R. Janson in *The Porphyrins: Physical Chemistry, Part C, Vol V*, ed D. Dolphin, Academic Press NY 1978, 401.

17. T.M. Cotton, P.A. Loach, J.J. Katz and K. Ballschmiter, *Photochem. Photobiol.*, **27**(1978), 735.

18. M. Kasha, H.R. Rawls and M. Ashraf El-Bayoumi, *Pure Appl. Chem.*, **11**(1965), 371.

19. L.L. Shipman, J.R Norris and J.J Katz , *J. Phys. Chem.*, **80**(1976), 877.

20. V.J. Koester, and F.K. Fong , *J. Phys. Chem.*, **80**(1976), 2310.

21. D.E. LaLonde, J.D. Petke and G.M Maggiora , *J. Phys. Chem.*,**92**(1988), 4746.

22. L.L. Shipman, T.M. Cotton, J.R. Norris and J.J. Katz, *Proc. Natl. Acad. Sci. USA*,**73**(1976), 1791.

23. D. Ben-Amotz and J.M. Drake, *J. Phys. Chem.*, **89**(1988), 1019.

24. M. Lee, A. Bain, C. Han, J. Haseltine, A. Smith III and R. Hochstrasser, *J. Chem. Phys.*, **85**(1986), 4341.

25. E. Åkesson, A. Hakkarainen, E. Laitinen, V. Helenius, T. Gillbro, J. Korppi-Tommola and V. Sundström, *J. Chem. Phys.*, **95**(1991), 6508.

26. J. Korppi-Tommola, A. Hakkarainen, T. Hukka and J. Subbi, *J. Chem. Phys.*, **95**(1991), 8482.

27. D. Ben-Amotz and T. W. Scott, *J. Chem. Phys.*, **87**(1987), 3739.

28. B.R. Brooks, R.E. Bruccoleri, B.D. Olafson, D.J. States, S. Swaminathan and M. Karplus , *J. Comp. Chem.*, 4(1983), 187.

29. H.-C. Chow, R. Serlin and C.E. Strouse, *J. Am. Chem. Soc.*, **97**(1975), 7230.

30. A.J. Alfano, F.E. Lyttle, M.S. Showell and F.K. Fong, *J. Chem. Phys.*, **82**(1985), 758.

31. V. Sundström, T. Gillbro, R.A. Gadonas and Piskarskas, *J. Chem. Phys,*. **85**(1988), 2574.

32. S.K. Rentsch, R.V. Danielius, R.A. Gadonas and A. Piskarskas, *Chem. Phys. Lett.* **84**(1981), 446.

33. A.E. Johnson, S. Kumazaki and K. Yoshihara, *Chem. Phys. Lett.* **211**(1993), 511.

34. T. Gillbro, Å. Sandström, M. Spangfort, V. Sundström and R. van Grondelle, *Biochim. Biophys. Acta,* **934**(1988), 369.

35. F.K. Fong, *Proc. Natl. Acad. Sci. USA*, **71**(1974), 3692.

36. R.J. Abraham, D.A. Goff and K.M. Smith , *J. Chem. Soc. Perkin Trans. I,* (1988), 2443.

37. S.G. Boxer and G.L. Closs, *J. Am. Chem. Soc.*, **98**(1976), 5406.

38. C. Houssier and K. Sauer, *J. Am. Chem. Soc.*, **92**(1970), 779.

39. R.P.H. Kooyman and T.J. Schaafsma, *J. Am. Chem. Soc.*, **106**(1984), 551.

40. P. Myslinski and J.A. Koningstein, *Chem. Phys.*, **161**(1992), 273.

41. S.J. Desjardins, L. Yixian, P. Myslinski, S. Yizhong and J.A. Koningstein, *J. Chem. Phys.*, **92**(1990), 4093.

42. D.L Thibodeau, J.A. Koningstein and L.V. Haley , *Chem. Phys.*, **138**(1989), 265.

43. F.K. Fong and V.J. Koester, *J. Am. Chem. Soc.*, **97**(1975), 6888.

44. F.K.Fong, *J. Am. Chem. Soc.*, **97**(1975), 6890.

45. R.J. Abraham and K.M. Smith, *J. Am. Chem. Soc.*, **105**(1983), 5734.

46. K. Ballschmiter and J.J. Katz , *J. Am. Chem. Soc.*, **91**(1969), 2661.

47. L. Stryer, *Biochemistry,* 3. ed., W.H. Freeman and Co., NY, 1988, 921.

48. R.S. Knox in *Rendiconti della Scuola Internazionale di Fisica - Enrico Fermi - XCVI Corso, Spettroscopia degli Stati Eccitati nei Solidi,* eds. UM. Grassano and N. Terzi, 1987, 481.

49. G. Careri, U. Buontempo, F. Carta, E. Gratton and A.C. Scott, *Phys. Rev. Lett.*, **51**(1983), 304.

50. G. Careri, U. Buontempo, F. Galluzzi, A.C. Scott, E. Gratton and E. Shyamsunder, *Phys. Rev.* **B30**(1984), 4689.

51. A.C. Scott, E. Gratton, E. Shyamsunder and G. Careri, *Phys. Rev.* **B32**(1985), 5551.

52. G. Careri, E. Gratton and E. Shyamsunder, *Phys. Rev.* **A37**(1988), 4048.

53. A.C. Scott, I.J. Bigio and C.T. Johnston, *Phys. Rev.* **B39**(1989), 12883.

54. D.M. Alexander, *Phys. Rev. Lett,* **54**(1985), 138.

55. D.M. Alexander and J.A. Krumhansl, *Phys. Rev.* **B33**(1986), 7172.

56. T. Holstein, *Ann. Phys.,* **8**(1959), 325.

57. S. Takeno, *Prog. Theor. Phys.,* **71**(1984), 395; **73**(1985), 853; **75**(1986), 1.

58. D.B. Fitchen in *Physics of Color Centers,* ed. W.B. Fowler, Academic Press, NY, 1968.

59. R.Lohikoski, *Excitation Transport in Helical Proteins: Dynamics of the Davydov-Scott Equations in the Adiabatic Approximation,* Phil. Lic. Thesis, Department of Physics, Laboratory Report 3/1992, University of Jyväskylä.

60. A.S. Davydov, *Biology and Quantum Mechanics,* Pergamon Press, 1982.

61. A.C. Scott, *Physica Scripta,* **29**(1984), 279.

62. B. Mechtly and P.B. Shaw, *Phys. Rev.* **B38**(1988), 3075.

63. A.C. Scott, *Phys. Rev.* **A26**(1982), 578.

64. B.M. Pierce in *Davydov's Soliton Revisited,* eds. P.L. Cristiansen and A.C. Scott, Plenum Press, NY, 1990.

65. D.L. Massart, B.G.M. Vandeginste, S.N. Deming, Y. Michotte and L. Kaufman, *Chemometrics: a textbook,* Elsevier, Amsterdam, 1988.

66. A.M. Dwivedi and S. Krimm, *Biopolymers,* **23**(1984), 923.

67. T. Miyazawa, *J. Mol. Spectrosc.,* **4**(1960), 168.

68. J.F. Rabolt, W.H. Moore and S. Krimm, *Macromolecules,* **10**(1977), 1065.

69. S. Krimm and A.M. Dwivedi, *J. Raman. Spectrosc.,* **12**(1982), 133.

70. A.C. Scott, *Physica,* **D51**(1991), 333.

ORIGINAL PAPERS

PAPER I

Computers. Chem. **16**(1992), 77-79

https://doi.org/10.1016/0097-8485(92)85012-N

PAPER II

Laser Spectroscopy of Biomolecules, Proc. SPIE **1921**(1993), 86-93

https://doi.org/10.1117/12.146105

PAPER III

Photochem. Photobiol. **58**(1993), 00-00
(Proof)

https://doi.org/10.1111/j.1751-1097.1993.tb04985.x

PAPER IV

(Manuscript)

https://doi.org/10.1016/0009-2614(94)00693-8

PAPER V

(Manuscript)

https://doi.org/10.1016/S0009-2614(97)01109-3